**Proceedings of the ASME 2010 3rd Joint US-European Fluids Engineering Summer Meeting and 8th International Conference on Nanochannels, Microchannels, and Minichannels**
**FEDSM-ICNMM2010**
**August 1-5, 2010, Montreal, Canada**

# FEDSM-ICNMM2010-30320

## Models for Gaseous Slip Flow in Circular and Noncircular Microchannels

**Zhipeng Duan** and **M.M. Yovanovich**
Department of Mechanical and Mechatronics Engineering, University of Waterloo
Waterloo, ON, N2L 3G1, Canada

### ABSTRACT

Slip flow in noncircular microchannels has been examined and a simple model for normalized Poiseuille number is proposed to predict the friction factor and Reynolds number product *fRe* for slip flow. The developed model for normalized Poiseuille number has an accuracy of 4.2 percent for all common duct shapes. As for slip flow, no solutions or graphical and tabulated data exist for most geometries, the developed simple model can be used to predict friction factor, mass flow rate, and pressure distribution of slip flow in noncircular microchannels for the practical engineering design of microchannels such as rectangular, trapezoidal, double-trapezoidal, triangular, rhombic, hexagonal, octagonal, elliptical, semielliptical, parabolic, circular sector, circular segment, annular sector, rectangular duct with unilateral elliptical or circular end, annular, and even comparatively complex doubly-connected microducts.

**Keywords:** Slip Flow, Microchannels, Noncircular Ducts, Poiseuille number, Pressure Distribution, Mass Flow Rate, Compressibility, Rarefaction

### NOMENCLATURE

| | | |
|---|---|---|
| $A$ | = | flow area, m$^2$ |
| $A_i$, $A_o$ | = | inner and outer areas, m$^2$ |
| $a$ | = | major semi-axis of ellipse or rectangle, m |
| $a$ | = | base width of a trapezoidal, triangular, double-trapezoidal, or rhombic duct, m |
| $b$ | = | minor semi-axis of ellipse or rectangle, m |
| $b$ | = | height of a trapezoidal, triangular, double-trapezoidal, or rhombic duct, m |
| $c$ | = | short side of a trapezoidal or double-trapezoidal duct, m |
| $D$ | = | diameter of circular tubes, m |
| $D_h$ | = | hydraulic diameter, $= 4A/P$ |
| $E(e)$ | = | complete elliptical integral of the second kind |
| $e$ | = | eccentricity, $= \sqrt{1 - b^2/a^2}$ |
| $f$ | = | Fanning friction factor, $= \tau / \left(\frac{1}{2}\rho\overline{w}^2\right)$ |
| $Kn$ | = | Knudsen number, $= \lambda \Big/ \left(\sqrt{\varepsilon}\sqrt{A}/2\right)$ |
| $L$ | = | channel length, m |
| $\mathcal{L}$ | = | arbitrary length scale, m |
| $\dot{m}$ | = | mass flow rate, kg/s |
| $m^*$ | = | normalized mass flow rate |
| $N$ | = | number of sides of a polygon |
| $n$ | = | correlation parameter |
| $P$ | = | total wetted perimeter, m |
| $Po$ | = | Poiseuille number, $= \overline{\tau}\mathcal{L}/\mu\overline{w}$ |
| $p$ | = | pressure, $N/m^2$ |
| $R$ | = | specific gas constant, $J/kg\,K$ |
| $Re$ | = | Reynolds number, $= \overline{w}\,\mathcal{L}/\nu$ |
| $r$ | = | dimensionless radius ratio, $= r_i/r_o$ |
| $r_i$ | = | inner radius of a concentric duct, m |
| $r_o$ | = | outer radius of a concentric duct, m |
| $T$ | = | temperature, K |
| $w$ | = | velocity, m/s |
| $\overline{w}$ | = | average velocity, m/s |
| $x$, $y$ | = | Cartesian coordinates, m |
| $z$ | = | coordinate in flow direction, m |

***Greek symbols***

| | | |
|---|---|---|
| $\alpha$ | = | parameter |
| $\beta$ | = | dimensionless slip parameter, $= Kn(2-\sigma)/\sigma$ |
| $\delta_n$ | = | eigenvalues |
| $\varepsilon$ | = | effective aspect ratio |
| $\lambda$ | = | molecular mean free path, m |
| $\mu$ | = | dynamic viscosity, $Ns/m^2$ |
| $\nu$ | = | kinematic viscosity, m$^2$/s |
| $\rho$ | = | density, kg/m$^3$ |
| $\sigma$ | = | tangential momentum accommodation coefficient |
| $\tau$ | = | mean wall shear stress, $N/m^2$ |

| | | |
|---|---|---|
| $\Omega$ | = | half angle of annular sector, rad |
| $\Phi$ | = | normalized Poiseuille number |

***Subscripts***

| | | |
|---|---|---|
| $\sqrt{A}$ | = | based upon the square root of flow area |
| $D_h$ | = | based upon the hydraulic diameter |
| $i$ | = | inlet |
| $\mathcal{L}$ | = | based upon the arbitrary length $\mathcal{L}$ |
| $ns$ | = | no-slip |
| $o$ | = | outlet |

## I. INTRODUCTION

Fluid flow in microchannels has emerged as an important research area. This has been motivated by their various applications such as medical and biomedical use, computer chips, and chemical separations. The advent of Micro-Electro-Mechanical Systems (MEMS) has opened up a new research area where non-continuum behavior is important. MEMS are one of the major advances of industrial technologies in the past decades. MEMS refer to devices which have a characteristic length of less than 1 mm but greater than 1 μm, which combine electrical and mechanical components and which are fabricated using integrated circuit fabrication technologies. Micron-size mechanical and biochemical devices are becoming more prevalent both in commercial applications and in scientific research.

Microchannels are the fundamental part of microfluidic systems. In addition to connecting different devices, microchannels are also utilized as biochemical reaction chambers, in physical particle separation, in inkjet print heads, in infrared detectors, in diode lasers, in miniature gas chromatographs, or as heat exchangers for cooling computer chips. Understanding the flow characteristics of microchannel flows is very important in determining pressure distribution, heat transfer, and transport properties of the flow. The characteristic dimension associated with the term “microchannels” is ambiguous. Nominally, microchannels may be defined as channels whose characteristic dimensions are from one micron to one millimeter. Typical applications may involve characteristic dimensions in the range of approximately 10 to 200 μm. Generally, above one millimeter the flow exhibits behavior which is the same as no-slip flows. The noncircular cross sections such as rectangular, isosceles triangular, trapezoidal, double-trapezoidal, and rhombic, are common channel shapes that may be produced by microfabrication. These cross sections have wide practical applications in MEMS [1-5].

The Knudsen number ($Kn$) relates the molecular mean free path of gas to a characteristic dimension of the duct cross-section. Knudsen number is very small for continuum flows. However, for microscale gas flows where the gas mean free path becomes comparable with the characteristic dimension of the duct, the Knudsen number may be greater than 0.001. Microchannels with characteristic lengths on the order of 100 μm would produce flows inside the slip regime for gas with a typical mean free path of approximately 70 nm at standard conditions. The slip flow regime to be studied here is classified as $0.001 < Kn < 0.1$.

In the slip regime, intermolecular collisions become less frequent and molecules arriving at the solid surface are unable to come into equilibrium with the surface. As a result, the no-slip boundary conditions are not valid, and a kinetic boundary layer on the order of one mean free path [2, 6], known as the ordinary Knudsen layer, starts to become dominant between the bulk of the fluid and the wall surface. The flow in the Knudsen layer cannot be analyzed using the Navier-Stokes equations, and it needs special equations of Boltzmann. However, for $Kn \leq 0.1$, the contribution of the Knudsen layer is small since it covers less than 10% of the channel height. The Knudsen layer can be replaced by extrapolating the bulk gas flow towards the walls [2].

## II. LITERATURE REVIEW

Rarefaction effects must be considered in gases in which the molecular mean free path is comparable to the channel’s characteristic dimension. The continuum assumption is no longer valid and the gas exhibits non-continuum effects such as velocity slip and temperature jump at the channel walls. Traditional examples of rarefied gas flows in channels include low-density applications such as high-altitude aircraft or vacuum technology. The recent development of microscale fluid systems has motivated great interest in this field of study. Microfluidic systems must take into account non-continuum effects. There is strong evidence to support the use of Navier-Stokes and energy equations to model the slip flow problem, while the boundary conditions are modified by including velocity slip and temperature jump at the channel walls.

The small length scales commonly encountered in microfluidic devices suggest that rarefaction effects are important. For example, experiments conducted by Pfalher et al. [7, 8], Harley et al. [9], Choi et al. [10], Arkilic et al. [11, 12], Pong et al. [13], Liu et al. [14], Shih et al. [15], Wu et al. [16], Araki et al. [17], Zohar et al. [18], Jang and Wereley [19], Hsieh et al. [20] on the transport of gases in microchannels confirm that continuum analyses are unable to predict flow properties in micro-sized devices.

Arkilic et al. [11, 12] investigated helium flow through microchannels. The microchannels were 52.25 μm wide, 1.33 μm deep, and 7.5 mm long. The results showed that the pressure drop over the channel length was less than the continuum flow results. The friction coefficient was only about 40% of the theoretical values. The significant reduction in the friction coefficient may be due to the slip flow regime, as according to the flow regime classification by Schaaf and Chambre [21], the flows studied by Arkilic et al. [11, 12] are mostly within the slip flow regime, only bordering the transition regime near the outlet. When using the Navier-Stokes equations with a first-order slip flow boundary condition, the slip model with full tangential momentum accommodation ($\sigma = 1$) fit the experimental data well.

Araki et al. [17] investigated frictional characteristics of nitrogen and helium flows through three different trapezoidal microchannels whose hydraulic diameter is from 3 to 10 μm. The measured friction factor was smaller than that predicted by the conventional theory. They concluded that this deviation was caused by the rarefaction effects.

Liu et al. [14] has also proved that the solution to the Navier-Stokes equation combined with slip flow boundary conditions show good agreement with the experimental data in microchannel flow.

Shih et al. [15] used helium and nitrogen for the flow experiments over a Reynolds number range of 0.001 – 0.01. The friction coefficient is only 30-45% of the theoretical values. This significant reduction in the friction coefficient may be due to the slip and transition flow regimes, as the Knudsen number for the data ranges from 0.02 to 0.16. This is consistent with the results of Liu et al. [14] and Arkilic et al. [11, 12]. Shih et al. conducted that the mass flow rate was greater than conventional no-slip theory predicted. The data agreed very well with a first-order slip flow model.

Hsieh et al. [20] investigated the behavior of nitrogen gas flow in a 200 μm wide and 50 μm deep microchannel for Reynolds numbers between 2.6 and 89.4 and a value of the Knudsen number ranging from 0.001 to 0.02. The results were in good agreement with the solutions to the Navier-Stokes equation with first order slip boundary conditions.

Maurer et al. [22] conducted experiments for helium and nitrogen flow in 1.14 μm deep 200 μm wide shallow microchannels. Flowrate and pressure drop measurements in the slip and early transition regimes were performed for averaged Knudsen numbers extending up to 0.8 for helium and 0.6 for nitrogen. The authors also provided estimates for second-order effects and found the upper limit of slip flow regime as the averaged Knudsen number equals 0.3±0.1.

Aubert and Colin [23] studied slip flow in rectangular microchannels using the second-order boundary conditions proposed by Deissler [24]. In a later study, Colin et al. [25] presented experimental results for nitrogen and helium flows in a series of silicon rectangular microchannels. The authors proposed that the second-order slip flow model is valid for Knudsen numbers up to about 0.25.

Ewart et al. [26] measured mass flow rate of isothermal gaseous slip flow in microtubes. The measured values were compared with analytical solutions and satisfactory results were obtained. The authors show that the second order effects could exist for average Knudsen numbers larger than 0.1.

The analytical study of internal flows with slip previously has been confined to simple geometries. Kennard [27] studied internal flows with slip in the circular tube and parallel-plate channel. Ebert and Sparrow [28] performed an analysis to determine the velocity and pressure drop characteristics of slip flow in rectangular and annular ducts. Sreekanth [29] developed a second-order analytical model for slip flow in circular tubes and Mitsuya [30] proposed a second-order analytical model for parallel plates. Duan and Muzychka [31] investigated slip flow in elliptic microchannels.

A number of researchers have attempted to develop second-order slip models which can be used in the transition regime. However, there are large variations in the second-order slip coefficient. The lack of a universally accepted second-order slip coefficient is a major problem in extending Navier-Stokes equations into the transition regime [2,32]. As analytical models derived using the first-order slip boundary condition have been shown to be relatively accurate up to Knudsen numbers of approximately 0.1, the first-order slip boundary condition will be employed in this paper.

## III. SLIP FLOW MODELS

**Characteristic Length Scale**

One of the most fundamental problems in fluid dynamics is that of fully developed laminar flow in circular and noncircular channels under constant pressure gradient. Upon obtaining the velocity distribution $w(x, y)$ and mean velocity $\overline{w}$, the friction factor Reynolds number product may be defined using the simple expression denoted in some texts as the Poiseuille number [33,34]:

$$Po_{\mathcal{L}} = \frac{\tau \mathcal{L}}{\mu \overline{w}} = \frac{\left(-\frac{A}{P}\frac{dp}{dz}\right)\mathcal{L}}{\mu \overline{w}} = \frac{f \, \mathrm{Re}_{\mathcal{L}}}{2} \tag{1}$$

The factor 2 appears because the Fanning friction factor is employed. The above grouping $Po$ is interpreted as the dimensionless average wall shear stress. The mean wall shear stress may also be related to the pressure difference by means of the force balance

$$\tau P L = \Delta p A \tag{2}$$

From this relation the mean wall shear stress is obtained

$$\tau = \frac{\Delta p}{L}\frac{A}{P} \tag{3}$$

Using the method of scale analysis, we can examine the momentum equation and consider the various force balance. Considering the force balance between the friction and pressure forces for a long microchannel:

$$\frac{\overline{w}}{\mathcal{L}^2} \sim \frac{1}{\mu}\frac{\Delta p}{L} \tag{4}$$

Substituting the relation for $\tau$ and the scale for $\overline{w}$ gives the following scale for the Poiseuille number:

$$Po_{\mathcal{L}} \sim \frac{A}{P}\frac{1}{\mathcal{L}} \tag{5}$$

which is purely geometric because it depends on the cross-section area $A$, the perimeter $P$ and the arbitrary length scale $\mathcal{L}$.

For closure the geometric parameter $C_{\mathcal{L}}$ is introduced so that

$$Po_{\mathcal{L}} = C_{\mathcal{L}}\frac{A}{P}\frac{1}{\mathcal{L}} \tag{6}$$

The geometric parameter $C_{\mathcal{L}}$ is found to depend on the geometry of the cross-section such as the shape, the aspect ratio, and the choice of the length scale $\mathcal{L}$.

The most frequently recommended length scale is the hydraulic diameter defined as

$$\mathcal{L} = D_h = \frac{4A}{P} = \frac{4\sqrt{A}}{P}\sqrt{A} \tag{7}$$

For this length scale the Poiseuille number becomes

$$Po_{D_h} = \frac{C_{D_h}}{4} \tag{8}$$

A novel length scale proposed by Muzychka and Yovanovich [34] is $\mathcal{L} = \sqrt{A}$. For this length scale the Poiseuille number becomes

$$Po_{\sqrt{A}} = C_{\sqrt{A}}\frac{\sqrt{A}}{P} \tag{9}$$

The grouping $P/\sqrt{A}$ is an important geometric scaling factor to describe fluid flow physical behavior.

In the fluid flow and heat transfer literature the convention is to use the hydraulic diameter. For circular tubes, the choice of the length scale in the definition of Reynolds number is obvious. However, for noncircular ducts, the question always arises of what to use as the correct length scale. Although it is customary to use the hydraulic diameter, this choice may be incorrect. The choice of a length scale with noncircular ducts has been a perennial and contentious issue. For noncircular geometries, it is desirable to eliminate or reduce the effects of geometry such that the general trends for all duct shapes may be easily modeled. It is better to choose an appropriate characteristic length scale to non-dimensionalize the fluid flow and heat transfer data. We will now examine the rectangular, elliptical and annular friction factor Reynolds number product results employing characteristic length $\sqrt{A}$ as Muzychka and Yovanovich [34], Duan and Muzychka [35], and Duan and Yovanovich [36] showed that the square root of the cross-sectional area was a more appropriate characteristic length scale than the hydraulic diameter for non-dimensionalizing the laminar no-slip and slip flow data.

**Rectangular Ducts**

We may now examine the solution for rectangular ducts for slip flow. Duan and Muzychka [35] presented the friction factor and Reynolds number product

$$f\,\mathrm{Re}_{\sqrt{A}} = \frac{2\left(-\dfrac{A}{P}\dfrac{dp}{dz}\right)\sqrt{A}}{\mu\overline{w}}$$

$$= \frac{2}{\sqrt{\varepsilon}(1+\varepsilon)\displaystyle\sum_{n=1}^{\infty}\frac{\varepsilon\sin^2\delta_n}{\delta_n^{\,4}\left(\delta_n+\sin\delta_n\cos\delta_n\right)}\left[\dfrac{\delta_n}{\varepsilon}-\dfrac{\sinh\left(\dfrac{\delta_n}{\varepsilon}\right)}{\cosh\left(\dfrac{\delta_n}{\varepsilon}\right)+\beta\delta_n\sinh\left(\dfrac{\delta_n}{\varepsilon}\right)}\right]} \tag{10}$$

where the eigenvalues, $\delta_n$, can be obtained from

$$\delta_n\tan\delta_n = \frac{1}{\dfrac{2-\sigma}{\sigma}\dfrac{\lambda}{b}} \tag{11}$$

The characteristic length scale for Knudsen number in the present analysis is defined as the smaller halfwidth of the cross-section $b$

$$Kn = \frac{\lambda}{b} = \frac{\lambda}{\dfrac{\sqrt{\varepsilon}}{2}\sqrt{A}} \tag{12}$$

Thus,

$$\delta_n\tan\delta_n = \frac{1}{\dfrac{2-\sigma}{\sigma}Kn} = \frac{1}{\beta} \tag{13}$$

where $\lambda$ is the molecular mean free path. The parameter $\sigma$ denotes tangential momentum accommodation coefficient, which is usually between 0.87 and 1 [37]. Although the nature of the tangential momentum accommodation coefficients is still an active research problem, almost all evidence indicates that for most gas-solid interactions the coefficients are approximately 1.0. The same procedure is valid even if $\sigma \neq 1$, defining a slip parameter as $\beta = Kn(2-\sigma)/\sigma$.

It can also be demonstrated that Eq. (10) reduces to its continuum flow limit as $\beta \rightarrow 0$:

$$\left(f\,\mathrm{Re}_{\sqrt{A}}\right)_{ns} = \frac{12}{\sqrt{\varepsilon}(1+\varepsilon)\left[1-6\displaystyle\sum_{n=1}^{\infty}\frac{\varepsilon}{\delta_n^{\,5}}\tanh\left(\frac{\delta_n}{\varepsilon}\right)\right]} \tag{14}$$

It was shown in [35] that the friction factor Reynolds number product *fRe* for slip flow in rectangular microchannels may be computed with reasonable accuracy by considering only the first term of the series in Eq. (10).

Considering only the first term of the series, Eq. (14) gives:

$$\left(f\,\mathrm{Re}_{\sqrt{A}}\right)_{ns} = \frac{12}{\sqrt{\varepsilon}(1+\varepsilon)\left[1-\dfrac{192\varepsilon}{\pi^5}\tanh\left(\dfrac{\pi}{2\varepsilon}\right)\right]} \tag{15}$$

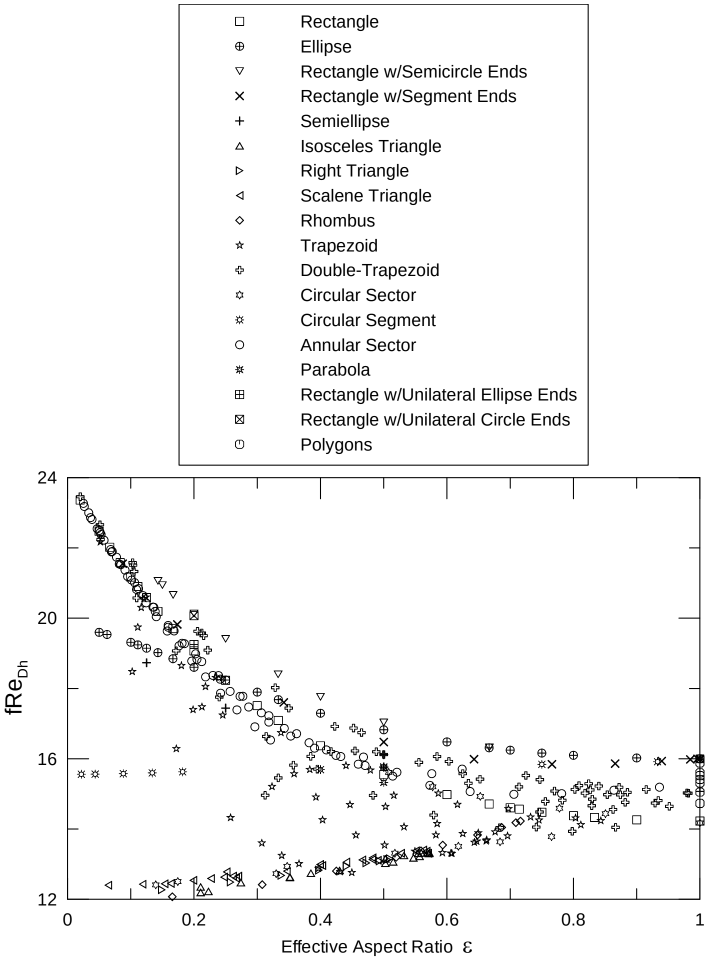


**Figure 1 Fully developed $f\,\mathrm{Re}_{D_h}$ for noncircular ducts**

Figures 1-5 [36] demonstrate that the square root of cross-sectional area is a more appropriate characteristic length scale than the hydraulic diameter for non-dimensionalizing the fully developed laminar flow data. The data for some noncircular ducts reported as $f\,\mathrm{Re}_{D_h}$ are plotted versus the effective aspect ratio ε in Figure 1. Some data increase with increasing values of ε while other data decrease with increasing values of ε. The definition of aspect ratio proposed by Muzychka and Yovanovich [34] and Duan and Yovanovich [36] is summarized in Table 1 for a number of geometries. The aspect ratio for regular polygons ($N \geq 4$) is unity. The aspect ratio for most singly connected ducts is taken as the ratio of the maximum width to maximum length such that $0 < \varepsilon < 1$. For the trapezoid duct, double-trapezoid duct, triangle duct, rhombic duct and the doubly connected duct, simple expressions have been derived to relate the characteristic dimensions of the duct to a width to length ratio. The next step in the comparisons is to convert all data from $f\,\mathrm{Re}_{D_h}$ to $f\,\mathrm{Re}_{\sqrt{A}}$ and re-plot versus the effective aspect ratio. When this is done as shown in Figure 2, all data follow closely a similar trend where the values decrease with increasing values of ε. Figure 3 shows the numerical data of *fRe* based on the hydraulic diameter for two families of doubly connected channels. When the length scale is changed to $\sqrt{A}$ as shown in Figure 4, all data follow the trend of the circular annulus which has a simple analytical solution. The large scatter in the data of Figure 3 vanishes when the length scale is changed from $D_h$ to $\sqrt{A}$ as seen in Figure 4. Finally, the data for all doubly connected channels are plotted as $f\,\mathrm{Re}_{\sqrt{A}}$ versus the effective aspect ratio as shown in Figure 5. The agreement is quite good. It was found that the use of the hydraulic diameter in laminar flow situations yields greater scatter in results as compared with the use of $\sqrt{A}$ as a characteristic length scale. When $\sqrt{A}$ is used, the effect of duct shape becomes minimized, and all of the laminar flow data can be predicted using a simple model based on the solution for the rectangular duct Eq. (15). This means that the dimensionless average wall shear stress can be made a weak function of duct shape. It is clear that Eq. (15) characterizes the fully developed laminar flow in noncircular ducts. The maximum deviation of exact values is less than 6.5%. The difference is much smaller and within 3% for most practical engineering configurations.

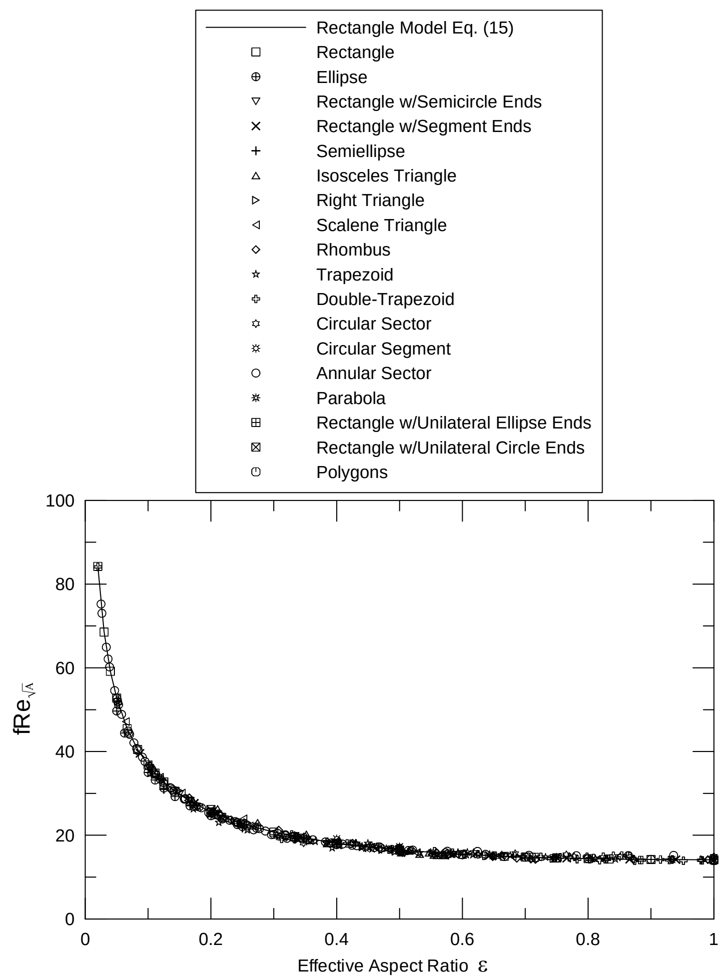


**Figure 2 Fully developed $f\,\mathrm{Re}_{\sqrt{A}}$ for noncircular ducts**

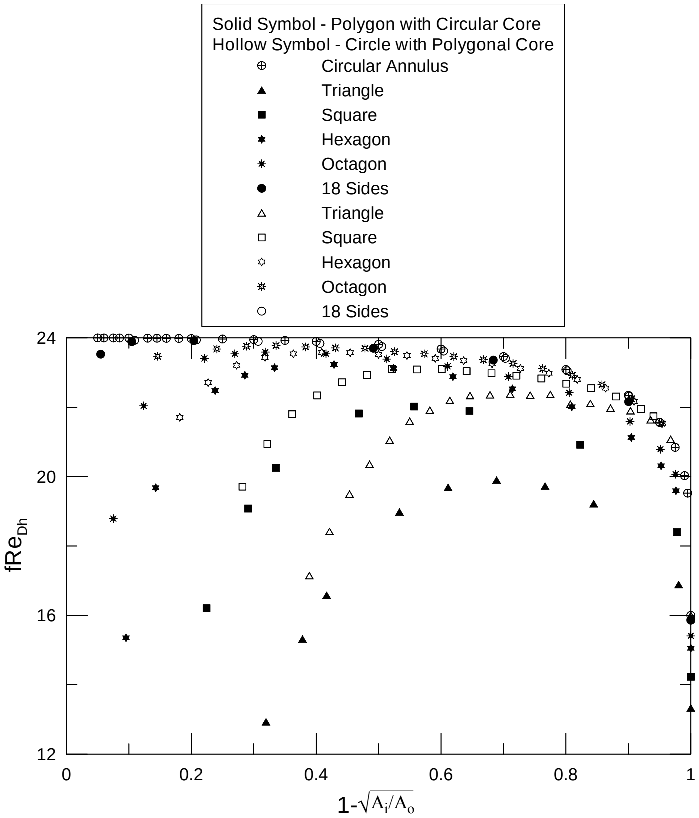


**Figure 3 Fully developed $f\,\mathrm{Re}_{D_h}$ for doubly connected ducts**

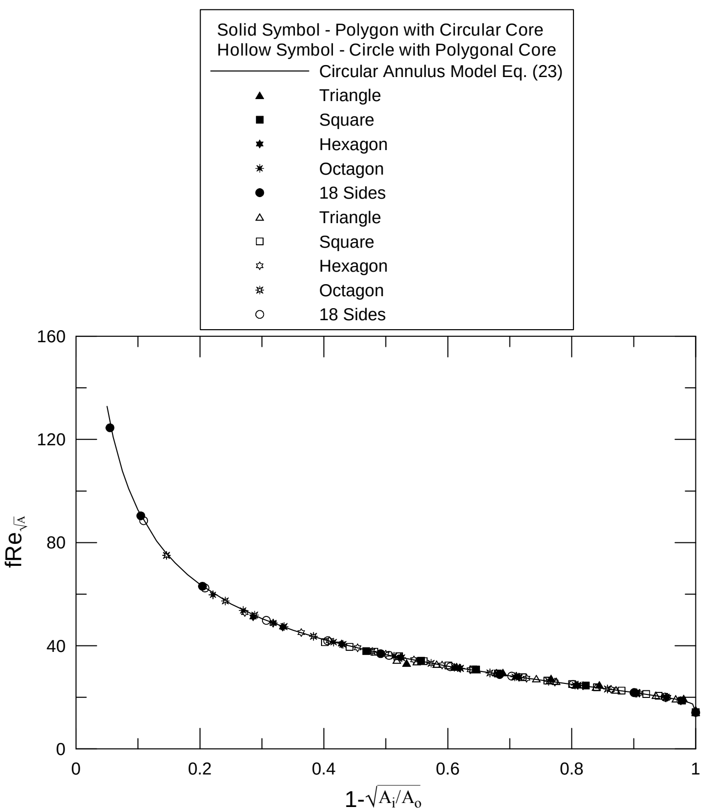


**Figure 4 Fully developed $f\,\mathrm{Re}_{\sqrt{A}}$ for doubly connected ducts**

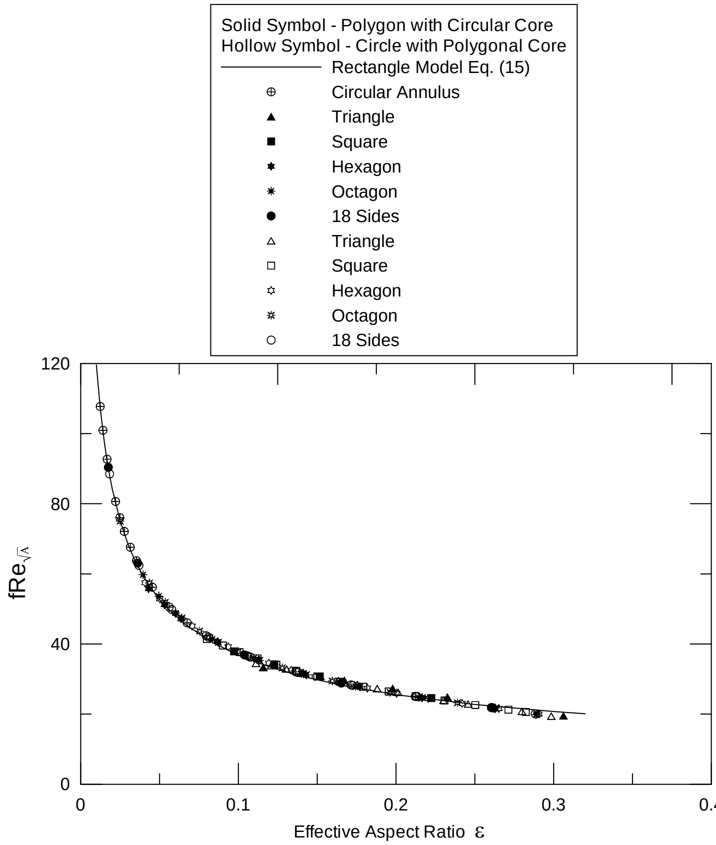


**Figure 5 Fully developed $f\,\mathrm{Re}_{\sqrt{A}}$ for doubly connected ducts**

**Table 1 Definitions of effective aspect ratio**

| Geometry | Effective Aspect Ratio |
|---|---|
| Regular Polygons | $\varepsilon = 1 \quad N \geq 4$ |
| Simple Singly-Connected | $\varepsilon = \dfrac{b}{a}$ |
| Trapezoid | $\varepsilon = \left[\left(\dfrac{2b}{a+c}\right)^n + \left(\dfrac{a+c}{2b}\right)^n\right]^{-1/n} \quad n = 1.7$ |
| Arbitrary Triangle | $\varepsilon = \left[\left(\dfrac{2b}{a}\right)^n + \left(\dfrac{2a}{b}\right)^n\right]^{-1/n} \quad n = 0.53$ |
| Double-Trapezoid | $\varepsilon = \left[\left(\dfrac{a+c}{2b}\right)^n + \left(\dfrac{1+\frac{c}{a}}{\frac{2a}{b}}\right)^n\right]^{-1/n} \quad n = 2.8$ |
| Rhombus | $\varepsilon = \left[\left(\dfrac{2b}{a}\right)^n + \left(\dfrac{2a}{b}\right)^n\right]^{-1/n} \quad n = 0.68$ |
| Circular Annulus | $\varepsilon = \dfrac{1-r}{\pi(1+r)}$ |
| Annular Sector | $\varepsilon = \dfrac{1-r}{\Omega(1+r)}$ |
| Doubly-Connected | $\varepsilon = \dfrac{1-\sqrt{A_i/A_o}}{\pi\left(1+\sqrt{A_i/A_o}\right)}$ |

The friction factor results can be presented conveniently in terms of normalized Poiseuille number. The Poiseuille number reduction depends on the geometry of the cross-section. It is convenient that the Poiseuille number results are expressible to good accuracy by the relation:

$$\Phi = \frac{Po}{Po_{ns}} = \frac{f\,\mathrm{Re}}{(f\,\mathrm{Re})_{ns}} = \frac{1}{1+\alpha\beta} \qquad (16)$$

A simple physical interpretation of $Po/Po_{ns}$ is based on the fact that the mean wall shear stress and the mean velocity are influenced by slip. It is given by

$$\frac{Po}{Po_{ns}} = \frac{(\text{mean wall shear stress with slip})/(\text{mean velocity with slip})}{(\text{mean wall shear stress without slip})/(\text{mean velocity without slip})} \qquad (17)$$

The parameter α should depend on ε and β for two-dimensional slip flows such as in rectangular microchannels.

We can solve for α given values of β and $Po/Po_{ns}$ from Eq. (16). Thus

$$\alpha = \frac{1}{\beta}\left(\frac{Po_{ns}}{Po} - 1\right) \qquad (18)$$

Calculated values of α for different values of ε and β are listed in Table 2. The values of α for a particular value of ε vary very slowly with β. For a given value of β, the values of α depend strongly on ε. It is clear that α is a weak function of β, and therefore it can be assumed that $\alpha = \alpha(\varepsilon)$. This was also observed for the ellipse and annulus solutions [31, 35].

**Table 2 The parameters α for different ε and β**

| ε | 0.1 | 0.3 | 0.5 | 0.6 | 0.7 | 0.8 | 0.9 | 1.0 |
|---|---|---|---|---|---|---|---|---|
| β | α | | | | | | | |
| 0.01 | 3.036 | 3.130 | 3.266 | 3.362 | 3.482 | 3.626 | 3.793 | 3.981 |
| 0.02 | 3.036 | 3.130 | 3.264 | 3.359 | 3.478 | 3.621 | 3.788 | 3.976 |
| 0.03 | 3.036 | 3.128 | 3.260 | 3.355 | 3.472 | 3.615 | 3.781 | 3.968 |
| 0.04 | 3.036 | 3.126 | 3.256 | 3.349 | 3.466 | 3.608 | 3.773 | 3.959 |
| 0.05 | 3.035 | 3.123 | 3.252 | 3.344 | 3.460 | 3.601 | 3.765 | 3.951 |
| 0.06 | 3.035 | 3.121 | 3.248 | 3.339 | 3.454 | 3.594 | 3.758 | 3.942 |
| 0.07 | 3.034 | 3.119 | 3.243 | 3.334 | 3.448 | 3.588 | 3.750 | 3.935 |
| 0.08 | 3.034 | 3.117 | 3.239 | 3.329 | 3.443 | 3.581 | 3.743 | 3.927 |
| 0.09 | 3.033 | 3.114 | 3.235 | 3.324 | 3.437 | 3.575 | 3.737 | 3.920 |
| 0.10 | 3.032 | 3.112 | 3.232 | 3.320 | 3.432 | 3.569 | 3.730 | 3.913 |
| 0.20 | 3.027 | 3.093 | 3.198 | 3.280 | 3.387 | 3.520 | 3.677 | 3.855 |

Since the parameters α are a function of aspect ratio and a weak function of β, the average values for each aspect ratio are fitted to a simple correlation as follows. It is found that the maximum error caused by using these constants in Eq. (19) is less than 1%. The error is much smaller and negligible for most cases

$$\alpha = 3.00 + 0.289\varepsilon + 0.135\varepsilon^2 + 0.508\varepsilon^3 \qquad (19)$$

Using Eqs. (16) and (19) we obtain:

$$\frac{Po}{Po_{ns}} = \frac{1}{1+\left(3.00 + 0.289\varepsilon + 0.135\varepsilon^2 + 0.508\varepsilon^3\right)\beta} \qquad (20)$$

Therefore, using the simple expression Eq. (20), the Poiseuille number results can be easily obtained to facilitate practical application for almost all common noncircular microchannels as follows:

$$f\,\mathrm{Re}_{\sqrt{A}} = \frac{1}{1+\alpha\beta}\,\frac{12}{\sqrt{\varepsilon}(1+\varepsilon)\left[1-\frac{192\varepsilon}{\pi^5}\tanh\left(\frac{\pi}{2\varepsilon}\right)\right]} \qquad (21)$$

The maximum difference between Eq. (21) and the exact solution for the rectangular duct Eq. (10) is less than 0.9%.

**Elliptical Ducts**

Duan and Muzychka [31] investigated slip flow in elliptic microchannels. An analytical solution of Poiseuille number was obtained using separation of variables in elliptic cylinder coordinates. Duan and Muzychka [31] developed a simple correlation for predicting the Poiseuille number in elliptic microchannels for slip flow:

$$\frac{Po}{Po_{ns}} = \frac{1}{1+\left(12.53 - 9.41\varepsilon + 4.87\varepsilon^2\right)\frac{E(e)}{2\sqrt{\pi}}\beta} \qquad (22)$$

**Annular Ducts**

Using a similar procedure as for rectangular ducts, it is not difficult to show that the no-slip friction factor Reynolds number product and the normalized Poiseuille number for an annular duct are as follows:

$$f\,\mathrm{Re}_{\sqrt{A}} = \frac{8\sqrt{\pi(1-r^2)}(1-r)}{1+r^2+\frac{1-r^2}{\ln r}} \qquad (23)$$

$$\frac{Po}{Po_{ns}} = \frac{1+r^2+\frac{1-r^2}{\ln r}}{1+r^2+2(r^2-r+1)\beta+\frac{r(1-r^2)(1+\beta)^2}{r\ln r-\frac{1}{2}(1-r^2)\beta}} \qquad (24)$$

where r = $r_i/r_o$ is the dimensionless radius ratio.

**Other Ducts**

Morini et al. [38] numerically studied the velocity distribution in microchannels with trapezoidal (with an apex angle ω = 54.74° imposed by the crystallographic morphology of the <100> silicon) and hexagonal (double-trapezoidal obtained by gluing together two trapezoidal channels) cross-section typical of microchannels. For the trapezoidal microchannels, the aspect ratio $b/a$ cannot exceed the value of $tg(\omega)/2$, corresponding to the degeneration of the isosceles triangular ducts. In the case of a double trapezoidal cross section, the aspect ratio $b/a$ ranges between 0 (parallel plates) and 1.414 (rhombic configuration). The channel height was employed as the length scale to define Knudsen number. The corresponding value of α for trapezoidal and double-trapezoidal microchannels was numerically determined and reported for different aspect ratios.

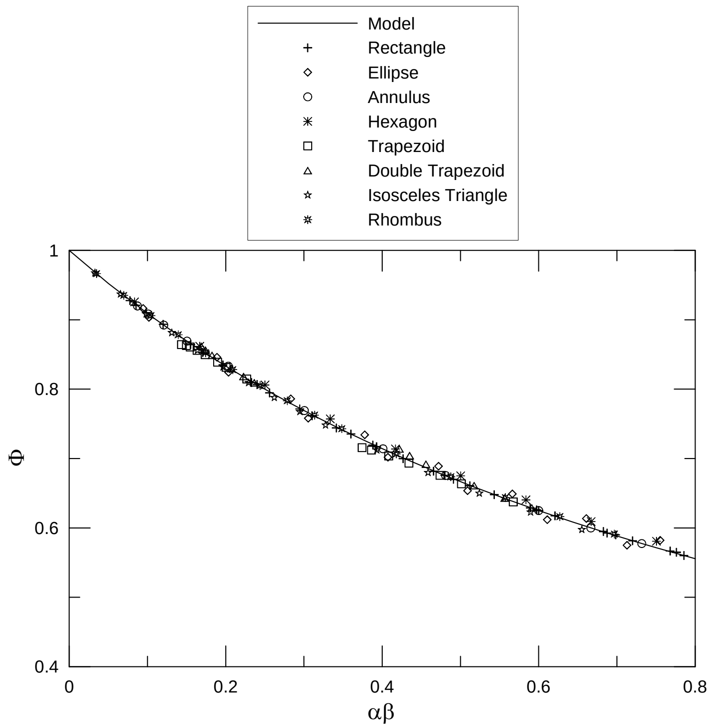


**Figure 6 comparison of the model for noncircular microchannels**

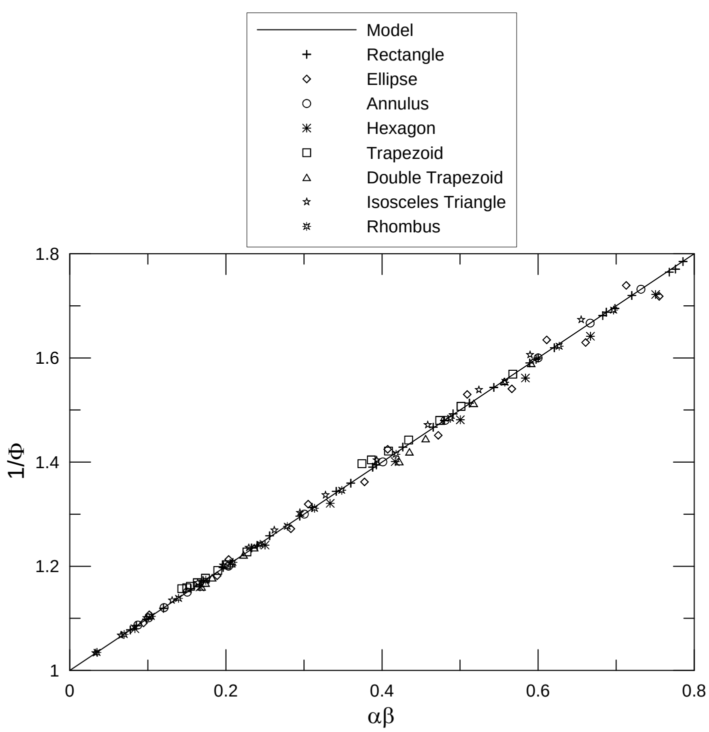


**Figure 7 comparison of the linear model for noncircular microchannels**

The simple model, Eq. (20), can also be applied to other common geometries. Figure 6 presents the comparison between the proposed simple model Eq. (20) and the analytical solution of elliptic ducts [31], rectangular and annular ducts [35], the numerical data of isosceles triangular, rhombic, trapezoidal, double-trapezoidal and hexagonal ducts [38]. The model predictions are in agreement with all the available slip flow data within 4.2%.

Furthermore, it is very convenient to express the Poiseuille number results by the following linear relation:

$$\frac{1}{\Phi} = \frac{Po_{ns}}{Po} = 1 + \alpha\beta \tag{25}$$

Figure 7 demonstrates the comparison between the proposed linear simple model Eq. (25) and all the available slip flow data. It is found that the model predictions agree with all the data very well (within 4.2%).

It is clear that Eq. (20) or Eq. (25) characterizes the noncircular microchannel slip flow. The maximum deviation of exact values is less than 4.2 percent. The friction factor Reynolds number product may be predicted from Eq. (20) or Eq. (25), provided an appropriate definition of the aspect ratio is chosen.

## IV. Mass Flow Rate and Pressure Distribution

Now, we take account of the compressibility of the gas. We treat compressible flow at low Mach numbers as a Navier-Stokes problem with slip. The flow is assumed to be locally fully developed and isothermal. The locally fully developed flow assumption means that the velocity field at any cross section is the same as that of a fully developed flow at the local density and the wall shear stress also takes on locally fully developed values. Compressibility effects enter through state equation and continuity equation. The mass flow rate in the microchannel is given by using the equation of state $p = \rho RT$, and the developed simple model $f\,\mathrm{Re}_{\sqrt{A}} = \left(f\,\mathrm{Re}_{\sqrt{A}}\right)_{ns} / \left(1+\alpha\beta\right)$. Combining these expressions yields:

$$\dot{m} = \rho\bar{w}A = \rho A \frac{2\left(-\dfrac{A}{P}\dfrac{dp}{dz}\right)\sqrt{A}}{\mu f\,\mathrm{Re}_{\sqrt{A}}} = -\frac{2\dfrac{A}{P}A\sqrt{A}}{\mu RT\left(f\,\mathrm{Re}_{\sqrt{A}}\right)_{ns}}\frac{dp}{dz}\,p\left(1+\alpha\beta\right) \tag{26}$$

We can use $p\beta = p_o\beta_o$ from kinetic theory of gases since $p\beta$ is constant for isothermal flow. After integrating Eq. (26) from $z = 0$ to local position $z$, we obtain:

$$\dot{m} = \rho\bar{w}A = \frac{p_o^2\dfrac{A^{5/2}}{P}}{\mu RTz\left(f\,\mathrm{Re}_{\sqrt{A}}\right)_{ns}}\left[\frac{p_i^2}{p_o^2} - \frac{p_z^2}{p_o^2} + 2\alpha\beta_o\left(\frac{p_i}{p_o} - \frac{p_z}{p_o}\right)\right] \tag{27}$$

Letting $z = L$ gives:

$$\dot{m} = \rho\bar{w}A = \frac{p_o^2 \frac{A^{5/2}}{P}}{\mu RTL\left(f\,\mathrm{Re}_{\sqrt{A}}\right)_{ns}}\left[\frac{p_i^2}{p_o^2}-1+2\alpha\beta_o\left(\frac{p_i}{p_o}-1\right)\right] \quad (28)$$

It is convenient to define the dimensionless mass flow rate as

$$m^* = \frac{\dot{m}\mu RTL\left(f\,\mathrm{Re}_{\sqrt{A}}\right)_{ns}}{p_o^2\frac{A^{5/2}}{P}} = \left[\frac{p_i^2}{p_o^2}-1+2\alpha\beta_o\left(\frac{p_i}{p_o}-1\right)\right] = \frac{2\Delta p}{p_o}\left(1+\frac{\Delta p}{2p_o}+\alpha\beta_o\right) \quad (29)$$

When the parameter $\Delta p/2p_o << 1$, the effect of compressibility is negligible. When $\alpha\beta_o << 1$, then the slip effect is negligible. When both parameters are sufficiently small, the general relation becomes

$$\dot{m} = \rho\bar{w}A = \frac{2\rho A^{5/2}\Delta p}{\mu PL\left(f\,\mathrm{Re}_{\sqrt{A}}\right)_{ns}} \quad (30)$$

which is the relation for flow of an incompressible fluid without slip.

The no-slip mass flow rate is given from Eq. (28):

$$\dot{m}_{ns} = \rho\bar{w}A = \frac{p_o^2\frac{A^{5/2}}{P}}{\mu RTL\left(f\,\mathrm{Re}_{\sqrt{A}}\right)_{ns}}\left(\frac{p_i^2}{p_o^2}-1\right) \quad (31)$$

The effect of slip may be illustrated clearly by dividing the slip flow mass flow Eq. (28) by the no-slip flow mass flow Eq. (31):

$$\frac{\dot{m}}{\dot{m}_{ns}} = 1+\frac{2\alpha\beta_o}{1+\frac{p_i}{p_o}} = 1+\frac{\alpha\beta_o}{1+\frac{\Delta p}{2p_o}} \quad (32)$$

It is seen that the rarefaction increases the mass flow and that the effect of rarefaction becomes more significant when the pressure ratio decreases.

The mass flow rate model Eq. (29) has been examined using experimental data by Arkilic et al. [12]. Figure 8 presents the normalized mass flow rate as a function of the pressure ratio. It is found that the predictions agree with experimental data by Arkilic et al. [12] within 9.8%. It is seen that there is a significant mass flow rate increase due to rarefaction effects from this Figure. The experimental data and model predictions are in good agreement.

Combining Eq. (27) and Eq. (28) and solving for $p_z/p_o$, we obtain the expression for pressure distribution in noncircular microchannels:

$$\frac{p_z}{p_o} = -\alpha\beta_o + \sqrt{\left(\alpha\beta_o+\frac{p_i}{p_o}\right)^2 - \left[\frac{p_i^2}{p_o^2}-1+2\alpha\beta_o\left(\frac{p_i}{p_o}-1\right)\right]\frac{z}{L}} \quad (33)$$

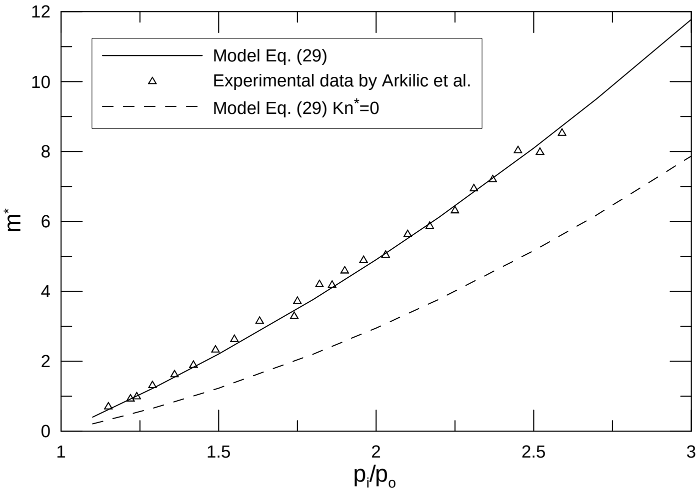


**Figure 8 Normalized mass flow rate comparison for experimental data by Arkilic et al. [12]**

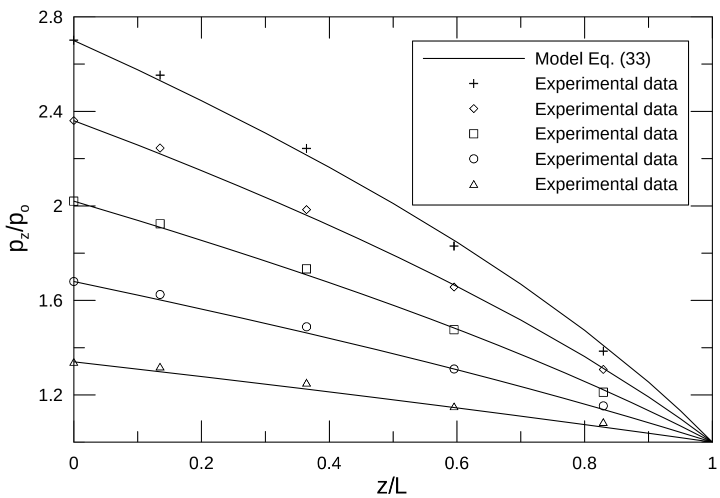


**Figure 9 Pressure distribution comparison for experimental data by Pong et al. [13]**

The pressure distribution exhibits a nonlinear behavior due to the compressibility effect. Pressure drop required is less than that in a conventional channel without slip. The deviations of the pressure distribution from the linear distribution decrease with an increase in Knudsen number. The nonlinearity increases as the pressure ratio increases. The effects of compressibility and rarefaction are opposite as Karniadakis et al. [2] demonstrated.

Figure 9 demonstrates the pressure distribution comparison between the proposed model Eq. (33) and experimental data by Pong et al. [13]. It is found that the model predictions agree with experimental data by Pong et al. [13] within 2.2%. From an inspection of this Figure, it is seen that when the pressure ratio is very small, the pressure distribution is nearly linear, which is close to an incompressible flow.

The deviations of the nonlinear pressure distribution from the linear distribution is given by:

$$\frac{p_z}{p_o}-\left[\frac{p_i}{p_o}-\left(\frac{p_i}{p_o}-1\right)\frac{z}{L}\right]$$
$$=-\alpha\beta_o+\sqrt{\left(\alpha\beta_o+\frac{p_i}{p_o}\right)^2-\left[\frac{p_i^2}{p_o^2}-1+2\alpha\beta_o\left(\frac{p_i}{p_o}-1\right)\right]\frac{z}{L}}-\frac{p_i}{p_o}+\left(\frac{p_i}{p_o}-1\right)\frac{z}{L} \quad (34)$$

Taking the derivative of Eq. (34) and setting it equal to zero, we obtain the location of the maximum deviation from linearity as

$$\frac{z}{L}=\frac{3\frac{p_i}{p_o}+4\alpha\beta_o+1}{4\left(\frac{p_i}{p_o}+2\alpha\beta_o+1\right)} \quad (35)$$

It is seen that the location of maximum deviation from linearity is between 0.5 and 0.75. The location approaches to 0.5 for low pressure ratio and approaches to 0.75 for high pressure ratio. The typical practical location of maximum deviation from linearity is between 0.5 and 0.6.

It may be pointed out that momentum changes are neglected in the above analysis for the pressure distribution and mass flow rate in microchannel flows. The effects of the momentum changes due to gas acceleration along the channel will become gradually important when the Mach number is increased. The effects of momentum changes on pressure distribution and mass flow rate have been analyzed by Duan [39,40].

## V. CONCLUSION

This paper investigated slip flow in noncircular microchannels. A simple model for normalized Poiseuille number was developed for predicting the friction factor Reynolds number product in noncircular microchannels for slip flow. The accuracy of the developed model for normalized Poiseuille number was found to be within 4.2 percent. As for slip flow no solutions or tabulated data exist for most geometries, this developed model can be used to predict Poiseuille number, mass flow rate, and pressure distribution of slip flow in noncircular microchannels such as rectangular, trapezoidal, double-trapezoidal, triangular, rhombic, hexagonal, octagonal, elliptical, semielliptical, parabolic, circular sector, circular segment, annular sector, rectangular duct with unilateral elliptical or circular end, annular, and even comparatively complex doubly-connected microducts.

These models are general and robust and can be used by the research community for practical engineering design of microchannel flow systems. The shape dependence has been minimized. The developed models will be extended to the transition regime by employing the second-order slip boundary conditions in another paper. A similar method can be applied to associated slip flow heat transfer problems in the future work. Also, due to the length restriction, the criterion for compressibility of gas flow in microchannels will be discussed in the future paper.

## ACKNOWLEDGMENTS

The authors acknowledge the support of the Natural Sciences and Engineering Research Council of Canada (NSERC).

## REFERENCES

[1] M. Ged-el-Hak, MEMS Handbook, CRC Press, 2001.
[2] G.E. Karniadakis, A. Beskok, N. Aluru, Microflows and Nanoflows, Springer, 2005.
[3] N.T. Nguyen, S.T. Wereley, Fundamentals and Applications of Microfluidics, Artech House, 2003.
[4] S.G. Kandlikar, S.V. Garimella, D. Li, S. Colin, M. King, Heat Transfer and Fluid Flow in Minichannels and Microchannels, Elsevier, 2006.
[5] D. Li, Encyclopedia of Microfluidics and Nanofluidics, Springer, 2008.
[6] C. Cercignani, Rarefied Gas Dynamics, Cambridge University Press, 2000.
[7] J. Pfahler, J. Harley, H. Bau, J.N. Zemel, Gas and liquid flow in small channels, Micromechanical Sensors, Actuators, and Systems ASME 32 (1991) 49-58.
[8] J. Pfahler, J. Harley, H. Bau, J.N. Zemel, Gas and liquid transport in small channels, Microstructures, Sensors and Actuators, ASME 19 (1990) 149-157.
[9] J. Harley, Y. Huang, H. Bau, J.N. Zemel, Gas flows in micro-channels, Journal of Fluid Mechanics 284 (1995) 257-274.
[10] S.B. Choi, R.F. Barron, R.O. Warrington, Fluid flow and heat transfer in microtubes, Micromechanical Sensors, Actuators, and Systems ASME 32 (1991) 123-134.
[11] E.B. Arkilic, K.S. Breuer, M.A. Schmidt, Gaseous flow in microchannels, Application of Microfabrication to Fluid Mechanics, ASME Vol. FED-197, 1994, pp. 57-66.
[12] E.B. Arkilic, K.S. Breuer, M.A. Schmidt, Gaseous slip flow in long microchannels, IEEE Journal of Microelectromechanical Systems 6 (2) (1997) 167-178.
[13] K. Pong, C. Ho, J. Liu, and Y. Tai, Nonlinear Pressure Distribution in Uniform Microchannels, *ASME Application of Microfabrication to Fluid Mechanics*, vol. FED-197, pp. 51-56, 1994.
[14] J. Liu, Y.C. Tai, C.M. Ho, MEMS for pressure distribution studies of gaseous flows in microchannels, in: IEEE International Conference on Micro Electro Mechanical Systems, Amsterdam, Netherlands, 1995, pp. 209-215.
[15] J.C. Shih, C. Ho, J. Liu, and Y. Tai, Monatomic and Polyatomic Gas Flow Through Uniform Microchannels, ASME Microelectromechanical Systems (MEMS), Vol. DSC-59, pp. 197-203, 1996.
[16] S. Wu, J. Mai, Y. Zohar, Y.C. Tai, C.M. Ho, “A suspended microchannel with integrated temperature sensors for high pressure flow studies,” in: Proceedings of IEEE Workshop on Micro Electro Mechanical Systems, Heidelberg, Germany, 1998, pp. 87-92.

 

[17] T. Araki, M.S. Kim, I. Hiroshi, K. Suzuki, An experimental investigation of gaseous flow characteristics in microchannels, in: G.P. Celata et al. (Eds.), Proceedings of International Conference on Heat Transfer and Transport Phenomena in Microscale, Begell House, New York, USA, 2000, pp. 155-161.
[18] Y. Zohar, S.Y. Lee, Y.L. Lee, L. Jiang, and P. Wong, Subsonic gas flow in a straight and uniform microchannel, Journal of Fluid Mechanics, vol. 472, pp. 125-151, 2002.
[19] J. Jang and S. T. Wereley, Pressure Distributions of Gaseous Slip Flow in Straight and Uniform Rectangular Microchannels, Microfluidics and Nanofluidics, vol. 1, pp. 41-51, 2004.
[20] S.S. Hsieh, H.H. Tsai, C.Y. Lin, C.F. Huang, and C.M. Chieh, Gas flow in a long microchannel, International Journal of Heat and Mass Transfer, vol. 47, pp. 3877-3887, 2004.
[21] S.A. Schaaf, P.L. Chambre, Flow of Rarefied Gases, Princeton Univ. Press, New Jersey, 1958.
[22] Maurer J, Tabeling P, Joseph P, Willaime H (2003) Second-order slip laws in microchannels for helium and nitrogen. Physics of Fluids 15:2613-2621.
[23] Aubert C, Colin S (2001) High-order boundary conditions for gaseous flows in rectangular microducts. Microscale Thermophysical Engineering 5:41-54.
[24] Deisler RG (1964) An analysis of second-order slip flow and temperature-jump boundary conditions for rarefied gases. International Journal of Heat and Mass Transfer, 7:681-694.
[25] Colin S, Lalonde P, Caen R (2004) Validation of a second-order slip flow model in rectangular microchannels. Heat Transfer Engineering 25:23-30.
[26] T. Ewart, P. Perrier, I Graur, J.G. Meolans, Tangential momentum accommodation in microtube, Microfluidics Nanofluidics, vol. 3, pp. 689-695, 2007.
[27] Kennard E.H., Kinetic Theory of Gases, McGraw-Hill, New York, 1938.
[28] W.A. Ebert, E.M. Sparrow, Slip flow in Rectangular and Annular Ducts, Journal of Basic Engineering, Vol. 87, 1965, pp. 1018-1024.
[29] Sceekanth, A., 1969. Slip flow through long circular tubes. In: Proceedings of the Sixth International Symposium on Rarefied Gas Dynamics, eds. Trilling L and Wachman HY, Academic Press, pp. 667-680.
[30] Y. Mitsuya, Modified Reynolds equation for ultra-thin film gas lubrication using 1.5-order slip-flow model and considering surface accommodation coefficient, J. Tribol., vol. 115, pp. 289-294, 1993.
[31] Z.P. Duan, Y.S. Muzychka, Slip flow in elliptic microchannels, International Journal of Thermal Sciences, vol. 46, pp. 1104-1111, 2007.
[32] Barber RW, Emerson DR (2006) Challenges in modeling gas-phase flow in microchannels: from slip to transition. Heat Transfer Engineering 27:3-12.
[33] S.W. Churchill, Viscous Flows: The Practical Use of Theory, Butterworth-Heinemann, Boston, MA, 1987.
[34] Y.S. Muzychka, M.M. Yovanovich, Laminar flow friction and heat transfer in non-circular ducts and channels: Part I-hydrodynamic problem, Compact Heat Exchangers, A Festschrift on the 60th Birthday of Ramesh K. Shah, Grenoble, France, 2002, pp. 123-130.
[35] Z.P. Duan, Y.S. Muzychka, Slip flow in noncircular microchannels, Microfluidics Nanofluidics, vol. 3, pp. 473-484, 2007.
[36] Z.P. Duan, and M.M. Yovanovich, Pressure drop for laminar flow in microchannels of arbitrary cross-sections, Semi-Therm 25 Semiconductor Thermal Measurement and Management Symposium, San Jose, CA, 2009, pp. 111-120.
[37] W.M. Rohsenow, H.Y. Choi, Heat, Mass, and Momentum Transfer, Prentice-Hall Inc., New Jersey, 1961.
[38] G.L. Morini, M. Lorenzini, M. Spiga, A criterion for experimental validation of slip-flow models for incompressible rarefied gases through microchannels, Microfluidics Nanofluidics 1 (2005) 190-196.
[39] Z.P. Duan, Analysis of slip flow in microchannels, Ph.D. dissertation, Memorial University of Newfoundland, St. John's, Newfoundland, Canada, 2007.
[40] Z.P. Duan, Y.S. Muzychka, Compressibility effect on slip flow in noncircular microchannels, Nanoscale and Microscale Thermophysical Engineering, vol. 11, pp. 259-272, 2007.